Coupled Electromagnetic-Thermal Analysis for Predicting Traction Motor Characteristics According to Electric Vehicle Driving Cycle

Sung-Woo Hwang, Jun-Yeol Ryu, Jun-Woo Chin, Soo-Hwan Park, Dae-Kee Kim, and Myung-Seop Lim, *Member, IEEE*

***Abstract*—The accuracy of motor characteristics prediction according to driving cycle can be improved by taking temperature change of motor into account. From this point of view, this paper proposes a fast and accurate coupled analysis method. To calculate motor circuit parameters, electromagnetic finite element analysis (FEA) is used. The proposed method consists of two stages to exclude the time consuming FEA from repetitive process. In preprocess stage, the circuit parameters are stored as look-up tables (LUTs) considering motor temperature. Further, a technique that allows reducing the number of analyses is developed to consider a wide operating temperature range with less time consumption. In main process stage, the torque and voltage equations are solved using the circuit parameter LUTs. Among the solved motor characteristics, losses are applied to lumped parameter thermal network (LPTN) as heat sources to figure out thermal characteristics. Here, techniques including loss separation and thermal parameter tuning are introduced to improve both accuracy and speed of the LPTN. Since the computation of the characteristic equations and LPTN are fast, the iterative analysis at entire time steps of the driving cycle is facilitated. An example of the proposed method is presented using worldwide harmonized light vehicle test procedure (WLTP). Thereafter, the effectiveness of the method is discussed by comparison with conventional methods. Finally, the experimental verifications are conducted to validate the electromagnetic FEA and LPTN used in this study.**

***Index Terms*—Coupled analysis, driving cycle, electric vehicle, lumped parameter thermal network, traction motor.**

I. Introduction

OWING to significant demand for eco-friendly technologies and high performance, battery electric vehicles (BEVs) have gained popularity in the automotive industry [1,2]. However, compared to the conventional vehicles equipped with internal combustion engine, BEVs are inferior in terms of mileage [3]. Their short range is an intrinsic drawback that originates from the lower energy density of the battery as compared to fossil fuel. Therefore, extending their mileages is a major concern in BEV development. Although battery technology has a strong influence on mileage, there are two other approaches to achieving it. First, many studies have focused on improving the efficiency of electric powertrain components (such as the electric motor, inverter, and converter) [4]–[6]. As the mileage of a BEV depends on its driving cycle, the efficiency of the motor should be investigated in consideration of motor operating pattern [7]. Second, many researchers are focusing on energy management strategies from the perspective of the entire system [8]–[10]. To establish an effective strategy, the characteristics of the electric motor, such as current and voltage, should be accurately predicted in accordance with the driving condition. In addition, the temperature of the motor needs to be managed to avoid thermal problems. In other words, both these approaches require accurate prediction of motor characteristics at each time step according to the driving cycle.

From this viewpoint, research has been conducted to analyze motor characteristics considering the vehicle driving cycle, [7], [11], [12]. In these studies, the time-varying temperature distribution of a traction motor is not considered, instead, the temperature of the motor is assumed to be a fixed value. Although this is a pragmatic approach with reasonable accuracy, there exists potential for higher accuracies if the temperature change is considered. In addition, it is difficult to determine an appropriate fixed value without experimentation. Many studies have considered electromagnetic and thermal fields. Nonetheless, some of these studies did not couple the two fields but only examined them separately [13]–[16]. A few studies coupled the fields using the trial and error method [17]–[21]. For the error of the parameter to be converged, many iterations are required for each time step. Hence, this type of method is not appropriate for predicting the characteristics at every step according to the driving cycle. In response to this problem, this paper proposes a fast and accurate coupled electromagnetic-thermal analysis method. The method is based on various theoretically simple but logically effective techniques.

Finite element analysis (FEA) is used for the electromagnetic field, while the lumped thermal parameter network (LPTN) is adopted for thermal field analysis [22]–[25]. This combination is selected to achieve high accuracy and low computational cost simultaneously. As mentioned previously, conducting

Manuscript received September 28, 2020; revised February 18, 2021; accepted March 29, 2021. Date of publication April 8, 2021; date of current version June 9, 2021. This work was supported by the National Research Foundation of Korea (NRF) funded by Korea government (MSIT) under Grant NRF2020R1A4A4079701. The review of this article was coordinated by Prof. J. Ye. *(Corresponding author: Myung-Seop Lim.)*

The authors are with the Department of Automotive Engineering, Hanyang University, Seoul 04763, South Korea (e-mail: supertramph@hanyang.ac.kr; jesus0925@hanyang.ac.kr; cjw1254@hanyang.ac.kr; shwanp14@hanyang.ac.kr; haunters@hanyang.ac.kr; myungseop@hanyang.ac.kr).

Digital Object Identifier 10.1109/TVT.2021.3071943

0018-9545 © 2021 IEEE. Personal use is permitted, but republication/redistribution requires IEEE permission.
See https://www.ieee.org/publications/rights/index.html for more information.

Authorized licensed use limited to: Hanyang University. Downloaded on June 17,2021 at 08:59:40 UTC from IEEE Xplore. Restrictions apply.

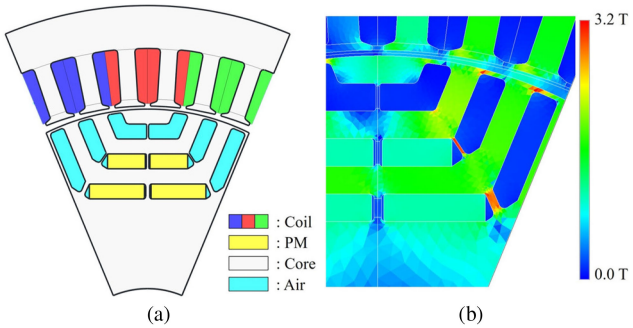

Fig. 1. Reference motor; configuration (left), flux density distribution at rated operating point (right).

TABLE I
SPECIFICATIONS OF THE REFERENCE MOTOR

Items	Unit	Value
Number of poles and slots	-	8 / 48
Stator outer diameter	mm	249
Rotor inner diameter	mm	60
Axial length	mm	177
Max. current	A_{pk}	480
DC link voltage	V_{DC}	400
Max. power	kW	160
Max. torque	Nm	400
Rated speed	rpm	3820
Max. speed	rpm	9500

electromagnetic FEA for every temperature condition inefficiently requires a significant amount of time. Therefore, a simple but effective technique is developed based on the behavior of the circuit parameters of the electric motor according to temperature. The temperature-dependent behavior of the circuit parameters is discussed in Section II. Using the proposed technique, the circuit parameter data obtained via FEA at just six temperature points was sufficient to accurately predict the characteristics of the motor from -40 to 160 °C. This temperature range was decided based on the traction motor specifications provided by the vehicle manufacturer. Using the pre-analyzed look-up table (LUT) of the circuit parameters, the motor voltage equation is solved to obtain the motor characteristics, including the losses. Subsequently, the losses are applied to the LPTN. This procedure, which consists of computation alone, is conducted at each time step according to the driving cycle. Consequently, the proposed method simultaneously achieves the well-known high accuracy of electromagnetic FEA and high speed over a wide temperature range. In addition, because the analysis results of a previous time step are applied to the next step, this approach provides highly accurate prediction when analyzing the time-varying load condition [26]. This process is discussed in further detail in Section III. For a higher accuracy temperature prediction, the LPTN for the multi-layered interior permanent magnet synchronous motor (IPMSM) is constructed. The thermal parameters of the LPTN, which are the most indistinct factor, are tuned based on experimental data by using the Gaussian process regression model [27].

An IPMSM for BEV traction was used as the reference model, as shown in Fig. 1(a). The specifications of the reference motor are presented in Table I. The model has a multi-layered arrangement of permanent magnets (PMs) and flux barriers in the rotor, thus, it undergoes harsh local magnetic saturation, which results in severe non-linearity. This harsh local magnetic saturation is demonstrated by the flux density distribution of the motor at rated operating point (400 Nm at 3820 rpm), as shown in Fig. 1(b). Therefore, the universality of the proposed method can be ensured by verifying the proposed method with the reference model. The reference model, is controlled with maximum torque per ampere (MTPA) method by an inverter using space vector pulse width modulation technique. The current harmonics caused by inverter switching were ignored in the analyses of this study. For the reference model, the characteristics according to the driving cycles are predicted using the proposed method. By comparing these results with those obtained via the conventional methods (where motor temperature is assumed to be a fixed value), the effectiveness of the proposed method is demonstrated. Finally, to validate the electromagnetic FEA, and the LPTN used in this study, experimental verifications were conducted.

II. TEMPERATURE-DEPENDENT BEHAVIOR OF CIRCUIT PARAMETERS OF IPMSM

When analyzing the electric motor characteristics, there are two factors that are affected by temperatures. First, the residual induction of the PM depends on temperature, and the circuit parameters of the electric motor, such as *d*- and *q*-axis inductances, flux linkage, and iron loss are dependent on the residual induction of the PM [28], [29]. Thus, the motor characteristics should be analyzed considering the given temperature. These circuit parameters are obtained with electromagnetic FEA [30]. As this is a considerably time-consuming procedure, a technique for reducing the computation time is required, instead of conducting FEA over the entire PM temperature range. Meanwhile, coil resistance, which is also a temperature-dependent factor, is not considered when performing the FEA. It is considered when solving the voltage equation, which is significantly faster than FEA. As an approach to reducing time consumption, this study aimed to minimize the number of temperature points at which FEA was conducted. Using the circuit parameters obtained at a few temperature points, their interpolated values were used at the other temperatures. The feasibility of using the interpolated values was demonstrated by investigating the trends of the parameters according to the temperature of the PM. The circuit parameters were calculated using FEA under various conditions, which cover the entire current range of the reference motor: amplitude of 10, 200, and 400 A_{rms}; phase of 0, 33, and 66°. The temperature-dependent behaviors are shown in Fig. 2. Within the operating range, all parameters exhibit monotonic trends according to the PM temperature. Although the *d*-axis inductance shows a relatively uneven trend, it is still sufficiently monotonic to use the spline-interpolated value. Fig. 3 shows the errors in the interpolated values. These interpolated

Authorized licensed use limited to: Hanyang University. Downloaded on June 17,2021 at 08:59:40 UTC from IEEE Xplore. Restrictions apply.

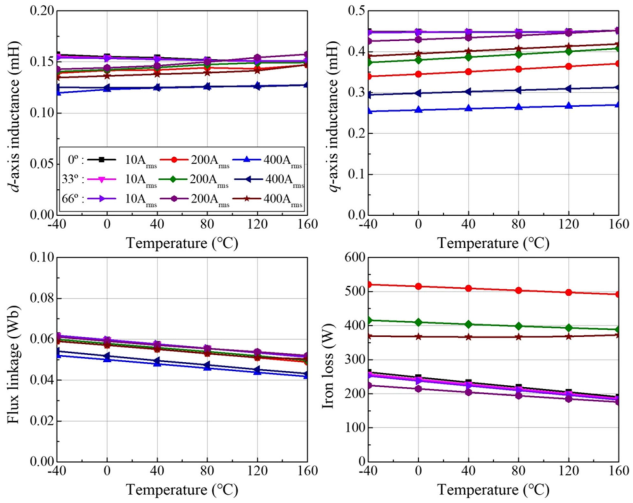

Fig. 2. Trends of circuit parameters according to temperature under various current conditions.

values at PM temperatures of -20, 60, and 140 °C were obtained from raw data analyzed at -40, 0, 40, 80, 120, and 160 °C via FEA. Those three comparison temperatures were determined considering that large error possibly occur at mid-points of raw data. Iron loss was calculated by multiplying the frequency term with the term of flux density in each element obtained via electromagnetic FEA [31]. Accordingly, it was found that the error is dependent not on the frequency but the current alone. Thus, the error map of the iron loss at a base speed of 4000 rpm, is presented. As expected from the trends in Fig. 2, the error in the *d*-axis inductance is the largest, among the other parameters. Nevertheless, its maximum error is less than 3%, which occurs at few points, and the overall error is less than 1%. Moreover, the errors in the other parameters are considerably smaller than those in the *d*-axis current. Consequently, it is concluded that using the interpolated values are reasonable.

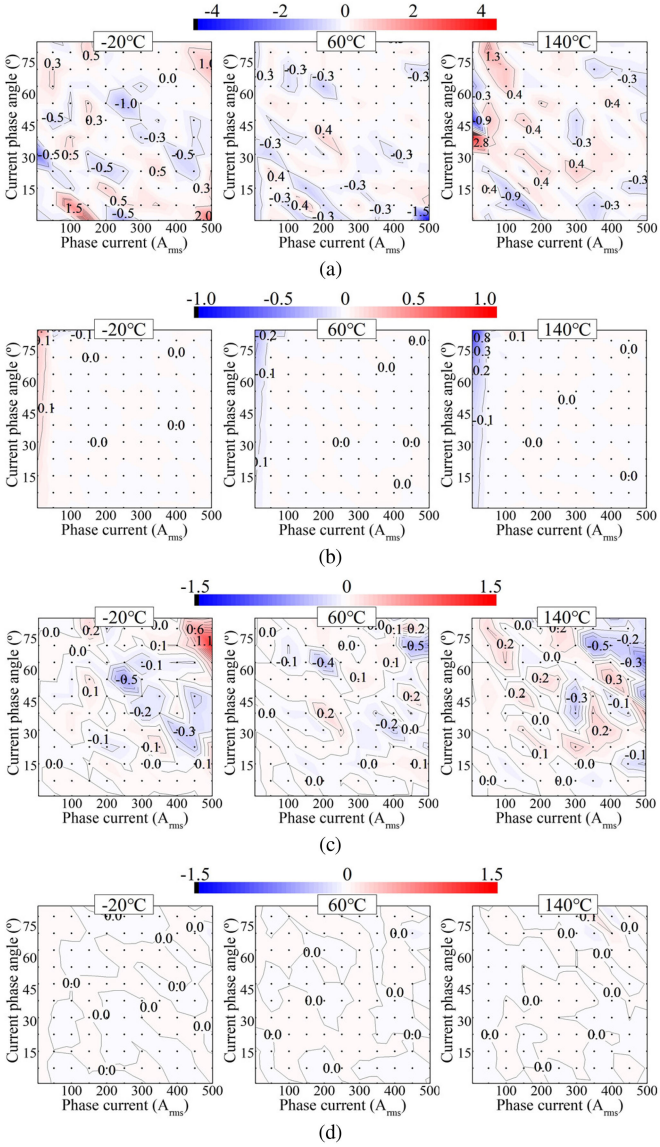

Fig. 3. Error maps of the circuit parameters interpolated according to PM temperature; (a) *d*-axis inductance (b) *q*-axis inductance (c) flux linkage (d) iron loss at base speed.

III. Proposed Coupled Electromagnetic-Thermal Analysis

Based on an investigation of the temperature-dependent behavior of circuit parameters, a method that enables the fast analysis of motor characteristics over a wide temperature range is developed. Including this technique, a process of the proposed coupled analysis is presented as follows.

A. Coupled Analysis Process

The process is divided into two stages; the pre-process and the main process, as shown in Fig. 4. Among the analysis methods used in entire process, FEA is the most time-consuming procedure. Therefore, FEA is performed in the pre-process, instead of being included in repetitive process. In the main process, motor characteristics and thermal analysis are iteratively conducted according to the time steps of the vehicle driving cycle. By isolating the most time-consuming procedure from the iterative process, total time cost is reduced. The types of analyses and their objectives are organized as below.

1) Pre-process
   -vehicle simulation: operating pattern of the motor according to a driving cycle is obtained
   -electromagnetic analysis: circuit parameters of the motor are calculated and stored as LUTs
2) Main process
   -motor voltage and torque equations: characteristics of motor are obtained using pre-analyzed LUTs
   -thermal analysis: LPTN is solved to acquire temperature change of motor

The pre-process is conducted to store two types of LUTs, which are used in the main process. To consider the vehicle driving cycle, vehicle simulation is performed. Using the

Authorized licensed use limited to: Hanyang University. Downloaded on June 17,2021 at 08:59:40 UTC from IEEE Xplore. Restrictions apply.

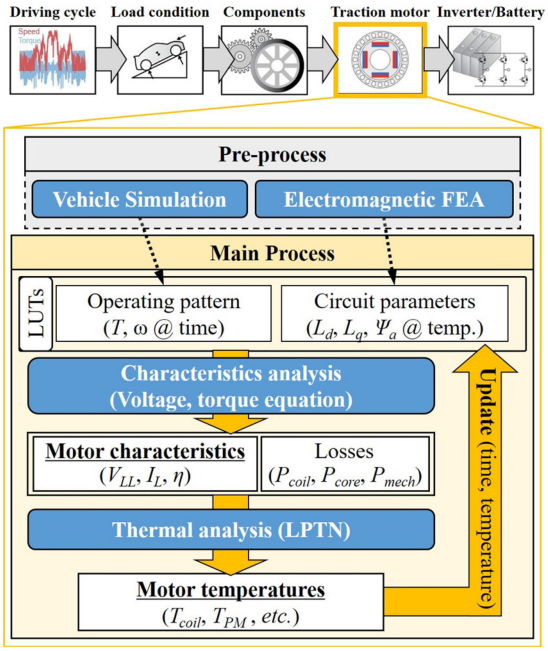

Fig. 4. Flow diagram of the proposed analysis process.

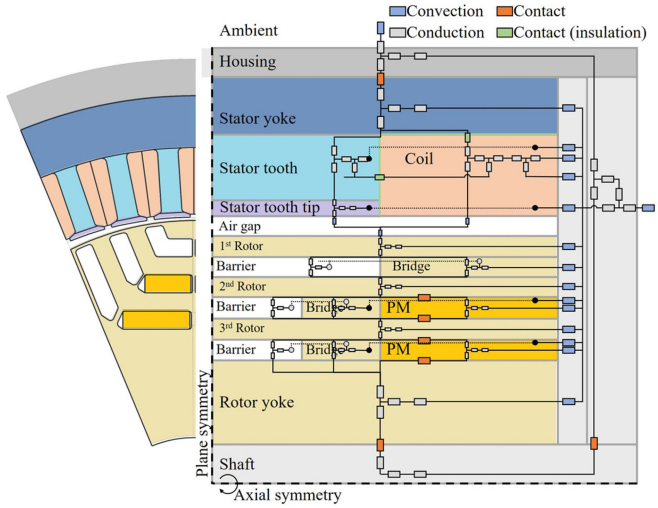

Fig. 5. LPTN model of multi-layered IPMSM (simplified).

driving cycle and the specifications of target vehicle, the LUT containing the motor operating pattern (i.e., desired torque and speed according to time) is obtained; The process of the vehicle simulation with an example is presented in Section IV. As well as, the LUTs of motor circuit parameters (i.e., d, q-axis inductances, flux linkage, and iron loss according to current and frequency) are acquired via FEA. As explained in Section II, those parameters are calculated at a few temperature points, and interpolated values are used to analyze motor characteristics. Considering that temperature of traction motor is changed over a wide range, the speed of whole analysis can be dramatically improved by this technique.

The main process contains the motor characteristic analysis and thermal analysis. Those two analyses are repeated at each time step of the motor operating pattern. The voltage and torque equations of IPMSM are used to analyze the motor characteristic, while the LPTN is used for the thermal analysis. Considering that computation of each equation is quite fast compared to FEA, it is appropriate to be included in the iterative process. The procedure of the motor characteristic analysis is explained in detail as follows. First, the circuit parameter LUTs are interpolated at a given temperature which is the initial temperature of the PM in the first time step. Thereafter, the motor characteristics are predicted using the interpolated circuit parameters. At this point, MTPA control method is applied for the motor to be operated at the desired torque and speed with least current draw and heat generation [32]. This procedure is performed by solving the d, q-axis voltage equation, and the torque equation of the IPMSM, as expressed in (1)-(3) [33].

$$\begin{bmatrix} v_d \\ v_q \end{bmatrix} = R_a \begin{bmatrix} i_{od} \\ i_{oq} \end{bmatrix} + \left(1 + \frac{R_a}{R_i}\right) \begin{bmatrix} v_{od} \\ v_{oq} \end{bmatrix} + \frac{d}{dt} \begin{bmatrix} L_d & 0 \\ 0 & L_q \end{bmatrix} \begin{bmatrix} i_{od} \\ i_{oq} \end{bmatrix} \tag{1}$$

$$\begin{bmatrix} v_{od} \\ v_{oq} \end{bmatrix} = \begin{bmatrix} 0 & -\omega L_q \\ \omega L_d & 0 \end{bmatrix} \begin{bmatrix} i_{od} \\ i_{oq} \end{bmatrix} + \begin{bmatrix} 0 \\ \omega \Psi_a \end{bmatrix} \tag{2}$$

$$T = P_n \left\{ \Psi_a i_{oq} + (L_d - L_q)\, i_{od} i_{oq} \right\} \tag{3}$$

Here, the subscripts d and q refer to the d- and q-axis components, respectively. The subscripts od and oq refer to the magnetization components of each variable. R_a and R_i refer to the armature resistance and equivalent iron loss resistance, respectively. v and i are the voltage and current, respectively; L is the inductance, $\omega$and Ψ are angular velocity and flux linkage, respectively; and T and P_n refer to the torque and number of pole pairs, respectively.

As a result, the electromagnetic motor characteristics, such as voltage, current, efficiency, copper loss, and iron loss, are determined. These parameters are stored according to the time step. Among the results, the losses are applied to the LPTN, because they act as heat sources, which are the input parameters of the LPTN. Using the LPTN for a period of the time step, the temperature distribution of the motor at the end of the present step is acquired. Among the results, the temperatures of the coil and the PM are applied to the analysis of the motor characteristics at the next time step. This procedure is iterated according to the entire driving cycle.

B. Techniques for LPTN Operation

The LPTN is based on the Mellor thermal network, which can efficiently model rotating machines with cylindrical shapes [34], [35]. Thus, the LPTN is widely used for thermal analyses because it reduces the time cost, and ensure reasonable accuracy [36], [37]. The validity of the LPTN has been demonstrated for various types of electric motors [38]–[41]. The LPTN model for the multi-layered IPMSM in this study is shown in Fig. 5. The geometrical elements and their heat transfer network are expressed considering the motor shape and assembly of each element. The

Authorized licensed use limited to: Hanyang University. Downloaded on June 17,2021 at 08:59:40 UTC from IEEE Xplore. Restrictions apply.

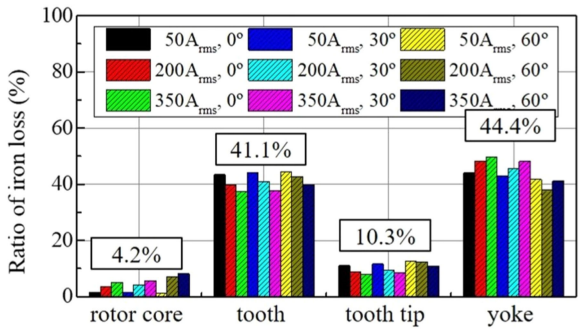

Fig. 6. Ratio of iron loss in each part under various current conditions.

effect of the coolant chiller was reflected as consistency in the coolant inlet temperature.

As mentioned above, the copper loss and iron loss are applied to the LPTN to predict the motor temperature in the next time step. These losses are separated to achieve a higher accuracy of the LPTN. The copper loss is simply separated into the coil side, and end coil by geometry with respect to their lengths. As their lengths remain constants regardless of the operating condition, the loss of each part can simply be obtained using the total copper loss and the ratio of their lengths. The iron loss is departmentalized into the stator yoke, tooth, tooth tip, and rotor, as shown in Fig. 5. Unlike the copper loss, the ratio of the iron loss in between parts is changed is not constant; this is because its main influencing factor, i.e., the flux density distribution of the iron core, depends on the current condition (i.e., the amplitude and phase angle). However, departmentalizing the iron loss at every condition requires additional computing time. Thus, the ratio of iron loss in each part is regarded as a constant, and it is used to calculate the separated iron loss from the entire iron loss of the motor, which is obtained via FEA. The validity of using a constant value for the iron loss ratio needs to be confirmed. The iron losses in each part under various current conditions were separated, and their ratios to the total iron loss are shown in Fig. 6. Overall, the difference according to the current condition of each part was small. Although the difference is large in the case of the rotor core, the amount is significantly less than the other loss [42]; hence, it can be considered as negligible. Therefore, each ratio is considered to remain constant, regardless of the current condition, in the proposed analysis method.

In addition to the losses, the thermal parameters have significant effect on the accuracy of the LPTN. Basically, the initial values of these parameters are determined empirically [43], [44]. Then they are tuned by fitting the analysis results to the measured data [45]. Depending on the method used for tuning the parameters, the tendency of the analyzed temperature varies. In other words, if the data are fitted focusing on the early phase, the error in the saturated temperature during the late phase increases, and vice versa. Thus, the approach adopted should depend on the aim of the fitting. In this study, the LPTN was used to predict motor temperature under time-varying load conditions. Therefore, fitting to short-term measured data was an appropriate solution. In this example, 150 s of measured data of the end coil and yoke temperature under three conditions were used. Among the many thermal parameters including the heat transfer coefficients, the 12 most uncertain and dominant ones were selected as variables: thermal conductivity of the coil insulation, air gap specific heat, five convection heat transfer coefficients, four thermal resistance coefficients, and coefficient of kinematic viscosity. The design of experiments was performed using the Latin hypercube sampling. Using the Gaussian process regression, the desirability function expressed in (4) was used for the multi-objective optimization.

$$\text{maximize } D = d_1^{w_1} \cdot d_2^{w_2} \cdots d_k^{w_k}, \ \sum_i^k w_i = 1 \qquad (4)$$

where D is the overall desirability, and d is the individual desirability. In the example of this study, there were six temperature data; at the end coil and stator yoke under three conditions. Each data was measured for 150 s. From each data, six individual desirability functions were extracted; five of the mean squared error (MSE) per each 30 s (i.e., 0-30 s, 30-60 s, etc.), and the final temperature at 150 s. Thus, the total number of individual desirability functions, k, is 36; six types of. By setting combinations of the weighting factor, w, for each individual desirability function, the optimal values for the thermal parameters were determined. The fitting results are presented in Section V, and compared with the measured data to validate the LPTN used in the proposed method.

TABLE II
SPECIFICATIONS OF THE TARGET VEHICLE

Items	Unit	Value
Type	-	Full electric SUV
Curb weight	kg	1685
Frontal area	m^2	2.83
Wheelbase	m	2.60
Wheel radius	mm	334
Max. speed	km/h	167
Gear ratio	-	7.981

IV. Prediction of Motor Characteristics According to Vehicle Driving Cycle

A. Motor Operating Pattern From Vehicle Driving Cycle

The first step is obtaining the operating pattern of the motor from a vehicle driving cycle considering the specifications of the target vehicle. In this example, a mass-produced fully electric sports utility vehicle was used and its specifications are presented in Table II. The vehicle simulation was performed using an advanced vehicle simulator (ADVISOR) [46]. To obtain the motor operating pattern, the vehicle simulation was carried out based on the worldwide harmonized light vehicle test procedure (WLTP). There are four categories in the WLTP depending on power-to-mass ratio and the maximum speed of the target vehicle. Class 3b of the WLTP, which is shown in Fig. 7(a), corresponds to the target vehicle. As the WLTP was established for a chassis dynamometer test to determine emissions and fuel consumption, all operating points of the motor are located within

Authorized licensed use limited to: Hanyang University. Downloaded on June 17,2021 at 08:59:40 UTC from IEEE Xplore. Restrictions apply.

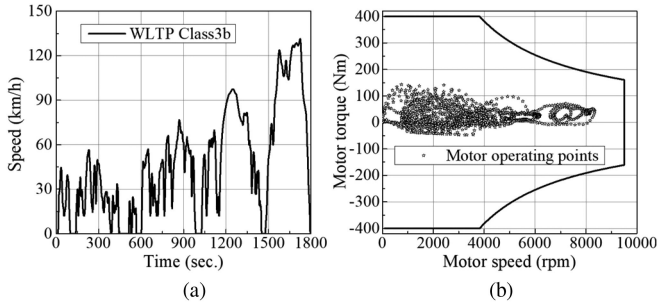

Fig. 7. Vehicle driving cycle (WLTP class 3b) and corresponding motor operating points.

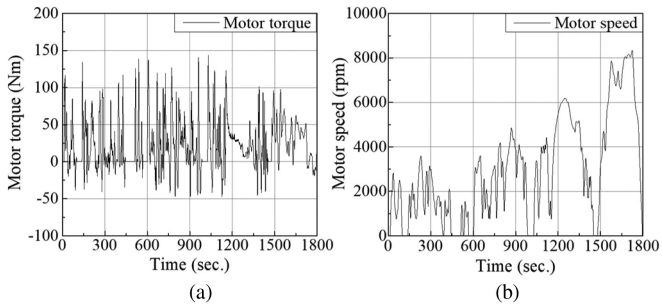

Fig. 8. Desired torque and speed of the motor according to time.

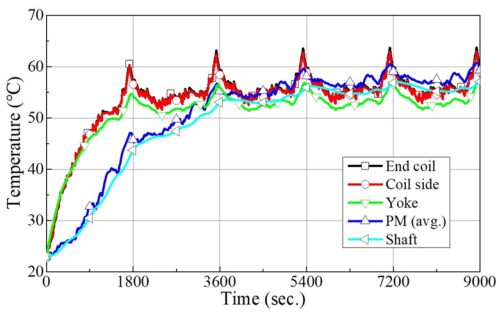

Fig. 9. Temperature trend of each part of the motor according to the 5 repeated vehicle driving cycle.

low torque and low power regions, as shown in Fig. 7(b). The points are spread over a wide speed range, but they barely reach one fourth of the maximum torque. Accordingly, harsh thermal variations of the motor were not expected. The desired torque and speed of the motor with respect to time are shown in Fig. 8. These were stored as the LUT of the motor operating pattern, and used in the main process at each time step.

B. Characteristics Prediction Results

The temperature trend of the reference motor equipped in the target vehicle was analyzed using the proposed method, as shown in Fig. 9. The analysis was repeated over five consecutive driving cycles. The ambient temperature and the time step were set as 23 °C and 1 s, respectively. As the reference motor is a multi-layered IPMSM, the average value of the four segments is used as the PM temperature. After the second cycle, the

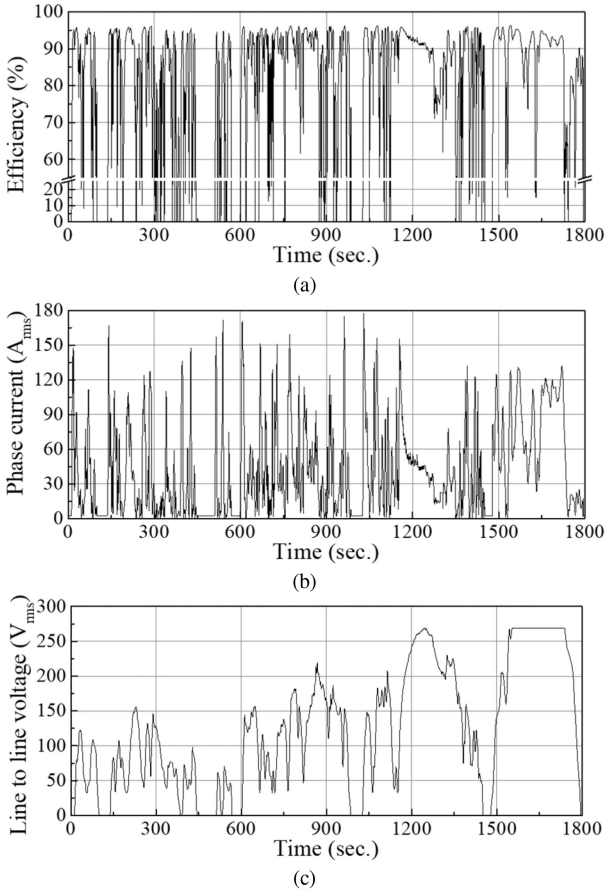

Fig. 10. Trends of the motor characteristics during a vehicle driving cycle.

temperature difference between the stator and the rotor parts is considerably small, while it is large in the early phase. Thus, it can be concluded that using the motor temperature as a lumped parameter is a potential cause of error when the analysis time is not sufficiently long. During the first driving cycle, the maximum differences between the highest and lowest temperatures are 24.1 °C for the coil and 38.2 °C for the PM. This is converted as a 9.5% increase in coil resistance and a 4.2% decrease in the residual induction of the PM. Low residual induction leads to a higher input current. A higher current and higher resistance result in a lower efficiency. The electromagnetic characteristics considering the temperature change are shown in Fig. 10. As the WLTP cycle does not aim for severe driving conditions, the reference motor is mostly operated under high-efficiency conditions, as shown in Fig. 10(a). In other words, the loss is so small that the overall efficiency is not affected significantly by the temperature under the WLTP Class 3b cycle. Furthermore, the trends of the phase current and line-to-line voltage according to the time are shown in Fig. 10(b) and Fig. 10(c), respectively. As these are the loads of the battery, the predicted results can be used to establish the battery management strategy.

C. Effectiveness of Proposed Method

In conventional methods without coupled analyses, the motor temperature needs to be assumed as a fixed value. However, it

Authorized licensed use limited to: Hanyang University. Downloaded on June 17,2021 at 08:59:40 UTC from IEEE Xplore. Restrictions apply.

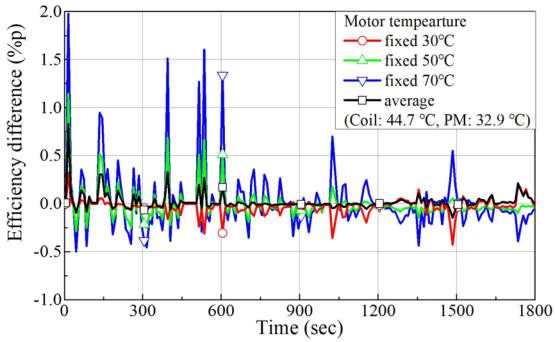

Fig. 11. Trends of efficiency difference between proposed and conventional methods; 4 types of conventional methods compared to proposed method.

is difficult to establish a criterion to determine the appropriate temperature. In addition, this inevitably causes accumulative errors. Thus, the empirical value or most severe condition is applied in general. The inaccuracy caused by neglecting the temperature change is shown in Fig. 11. The graphs depict the trends of efficiency differences between the conventional methods and the proposed method. The values are obtained using (5), where η is the predicted efficiency.

$$\eta_{\text{difference}} = \eta_{\text{proposed}} - \eta_{\text{conventional}} \tag{5}$$

The graph with data per 1 s, such as Fig. 10, is significantly uneven, making it difficult to review. Therefore, the graph with data averaged over 10 s is used, as shown in Fig. 11. There are four types of conventional methods. The red, green, and blue colored lines represent the conditions under which the motor temperature is assumed to be 30, 50, and 70 °C, respectively. It can be determined that the prediction accuracy varies depending on the assumed temperature. In addition, regardless of the PM temperature assumed, imprecise predictions will be obtained. The black line with rectangular symbols represents a condition in which the coil and PM temperatures are as 44.7 and 32.9 °C, respectively. These values were acquired by averaging the data in Fig. 9. As mentioned previously, this example presents the case with the low temperature dependency of efficiency. When a motor is analyzed over a long-term cycle, accumulative characteristics, such as the mileage of a vehicle, will be critically affected by temperature, even if it is a less temperature-dominant case.

V. Experimental Verification

To confirm the validity of the analysis methods used in the proposed process, experiment al verifications were conducted. The reference motor was controlled with MTPA control method by an inverter using space vector pulse width modulation technique. As the process includes the electromagnetic field analysis via FEA, and thermal field analysis via the LPTN, verifications were performed separately for each field. The experimental setup is shown in Fig. 12. To measure torque, a torque transducer, HBM T12 (maximum 1kNm, sensitivity tolerance ±0.1%), was

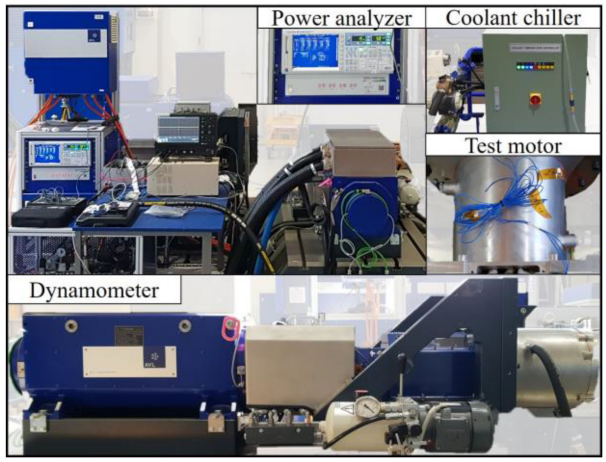

Fig. 12. Experimental setup for verification.

TABLE III
Comparison Conditions; Group A

Items		Unit	Conditions			
			1	2	3	4
Speed		rpm	2000	3820	5000	9500
Current	Amp.	A_{rms}	478.3	492.5	461.8	398.5
	Phase	°	49.4	55.9	66.6	77.6

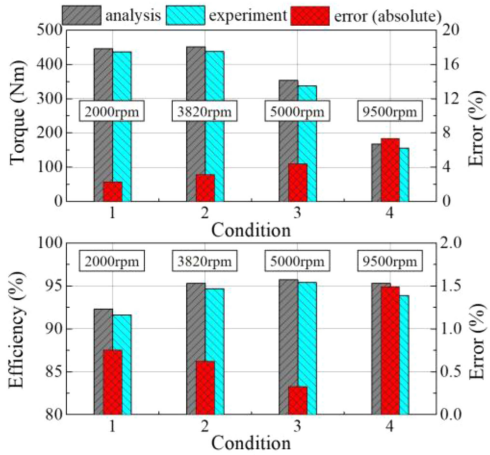

Fig. 13. Comparison between electromagnetic FEA and experiment results; Group A.

used. Electrical inputs, such as the line-to-line voltage and line current were analyzed using Yokogawa WT 3000.

A. Electromagnetic FEA

The load test for the verification of the electromagnetic FEA was performed at eight points. First, the four points of group A aimed the peak power of 160 kW, as shown in Table III, and comparison results of the torque and efficiency are shown in Fig. 13. The torque error in 2000 and 3820 rpm, which are constant torque region, were within reasonable level. While, the error increased as speed increased. It can be estimated that there

Authorized licensed use limited to: Hanyang University. Downloaded on June 17,2021 at 08:59:40 UTC from IEEE Xplore. Restrictions apply.

TABLE IV
COMPARISON CONDITIONS; GROUP B

Items		Unit	Conditions			
			1	2	3	4
Speed		rpm	2000	3410	6500	9500
Current	Amp.	A_{rms}	319.9	322.5	239.4	259.6
	Phase	°	41.2	41.5	60.6	73.9

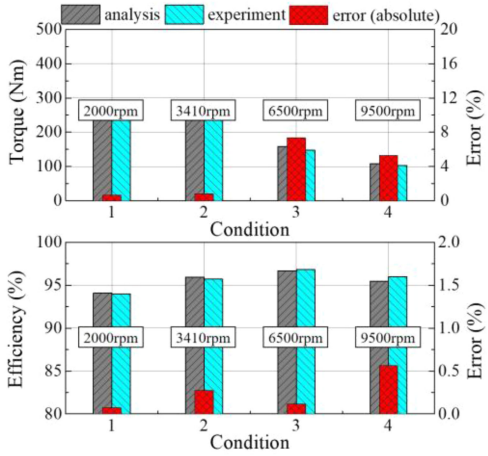

Fig. 14. Comparison between electromagnetic FEA and experiment results; Group B.

were error factors related to the frequency. Usually, assumption of the mechanical loss could be one of the frequency-related factor. In particular, a relatively larger error in the torque was noted at the maximum speed of 9500 rpm. Nevertheless, because the target motor is operated at speed lower than 9000 rpm under given driving cycle as shown in Fig. 7(b), the error in highest speed has negligible influence on the analyses conducted this study. Meanwhile, the efficiency results obtained by the FEA and experiment well agreed to each other over all speed range. For the largest efficiency error at 9500 rpm, the aforementioned factor, mechanical loss could be the reason. Second, the group B consists of four points with continuous operating conditions as shown in Table IV. Overall, errors were within allowable level, as shown in Fig. 14. In conclusion, the validity of the electromagnetic FEA used in this study was demonstrated.

B. Lumped Parameter Thermal Network

Thermal experiments were conducted under three conditions, as shown in Table V. As this motor is operated in the low power region under the target driving cycle, as shown in Fig. 7(b), the conditions of low and mid-power were selected. The flow rate of the coolant and the ambient temperature were the same for all conditions. Compared to condition 1, condition 2 aimed relatively lower power operation and the condition 3 was included for higher power operation. The temperature trends of the yoke and end coil were measured and compared to the analysis results of the LPTN, as shown in Fig. 15(a) and (b), respectively. Given that the error of condition 2 is the smallest and the error

TABLE V
CONDITIONS OF THERMAL EXPERIMENT

Items	Unit	Conditions		
		1	2	3
Power	kW	80	20	100
Torque	Nm	200	50	280
Speed	rpm	3820	3820	3410
Coolant flow rate	LPM		12	
Coolant inlet temperature	°C	50	30	50
Ambient temperature	°C	23	23	22

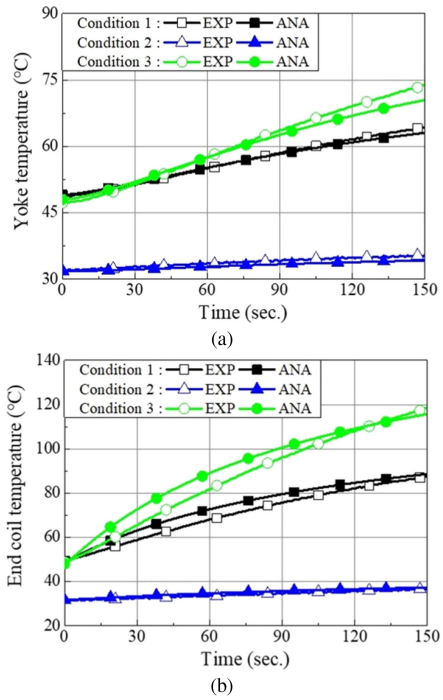

Fig. 15. Comparison between LPTN and thermal experiment results; (a) yoke temperature (b) end coil temperature.

of condition 3 is the largest, the prediction through the LPTN in this study can be regarded to be more accurate at lower torques. The error of the end coil temperature in the early state of condition 3 reached a maximum of almost 8 °C. However, this difference under the highest torque condition has less influence over the accuracy of prediction over the entire driving cycle. This is because the motor is mostly operated under lower torque conditions. In addition, overall, the predicted temperature was higher than the measured temperature. This can be regarded as a safety margin that prevents overheating. Consequently, the LPTN in this study can be regarded as being well composed, and its thermal parameters can be considered to be w ell tuned by the optimization process.

VI. CONCLUSION

To predict the characteristics of traction motor according to vehicle driving cycles, this paper proposed a coupled electromagnetic-thermal analysis method that is both accurate and significantly fast. In the pre-process, the operating pattern

Authorized licensed use limited to: Hanyang University. Downloaded on June 17,2021 at 08:59:40 UTC from IEEE Xplore. Restrictions apply.

of motor under given driving cycle were obtained via vehicle simulation using ADVISOR. Thereafter, electromagnetic FEA was conducted to acquire LUTs of motor circuit parameter which depend on the PM temperature. Here, temperature-dependent behavior of the circuit parameters was investigated to develop a technique allowing only a few number of FEA to cover a wide temperature range. In the presented example, a range from -40 to 160 °C was sufficiently covered with just 6 temperature points. This is one of contributions to reduce the time-cost of entire process. Its effectiveness is maximized in the case of traction motor whose operating range is considerably wide. In addition, by performing the FEA only in the pre-process and using only the LUTs in the main process, the speed was significantly improved. In the main process, the circuit parameters interpolated to a desired temperature were applied to the voltage and torque equation of PMSM to obtain motor characteristics. Through applying the losses from results of the characteristic analysis to the thermal analysis, the LPTN is coupled with electromagnetic field analysis. To improve the accuracy of the LPTN, losses were departmentalized considering the motor shape, and the thermal parameters were optimized using Gaussian process regression. The parameters were fitted considering that the motor is mostly operated at low torque region; one fourth of the maximum torque in the case of this study. Finally, the experimental verifications were performed for the electromagnetic FEA, and the LPTN.

The proposed coupled analysis method is expected to facilitate research on electric powertrains and strategy for the mileage extension of BEV. First, a motor control scheme for maximizing efficiency can be established by considering the variation in motor temperature according to the vehicle driving cycle. This consideration is also important in motor design. Second, precise predictions of the energy consumption of the motor would be useful for energy management strategies of the vehicle, such as adaptive regenerative braking. Furthermore, predicting the current draw of the motor would enable temperature management of the entire electric powertrain.

REFERENCES

[1] A. G. Boulanger, A. C. Chu, S. Maxx, and D. L. Waltz, "Vehicle electrification: Status and issues," *IEEE*, vol. 99, no. 6, pp. 1116–1138, Jun. 2011.

[2] B. Bilgin *et al.*, "Making the case for electrified transportation," *IEEE Trans. Transp. Electrific.*, vol. 1, no. 1, pp. 4–17, Jun. 2015, doi: 10.1109/TTE.2015.2437338.

[3] D. Gong, M. Tang, B. Buchmeister, and H. Zhang, "Solving location problem for electric vehicle charging stations—A sharing charging model," *IEEE Access*, vol. 7, pp. 138391–138402, 2019, doi: 10.1109/ACCESS.2019.2943079.

[4] J. Zhu, K. W. E. Cheng, X. Xue, and Y. Zou, "Design of a new enhanced torque in-wheel switched reluctance motor with divided teeth for electric vehicles," *IEEE Trans. Magn.*, vol. 53, no. 11, Nov. 2017, Art. no. 2501504, doi: 10.1109/TMAG.2017.2703849.

[5] K. Ahn, A. E. Bayrak, and P. Y. Papalambros, "Electric vehicle design optimization: Integration of a high-fidelity interior-permanent-magnet motor model," *IEEE Trans. Veh. Technol.*, vol. 64, no. 9, pp. 3870–3877, Sep. 2015, doi: doi: 10.1109/TVT.2014.2363144.

[6] G. Ma, M. Ghasemi, and X. Song, "Integrated powertrain energy management and vehicle coordination for multiple connected hybrid electric vehicles," *IEEE Trans. Veh. Technol.*, vol. 67, no. 4, pp. 2893–2899, Apr. 2018, doi: 10.1109/TVT.2017.2780268.

[7] A. Fatemi, D. M. Ionel, M. Popescu, Y. C. Chong, and N. A. O. Demerdash, "Design optimization of a high torque density spoke-type PM motor for a formula e race drive cycle," *IEEE Trans. Ind. Appl.*, vol. 54, no. 5, pp. 4343–4354, Sep./Oct. 2018, doi: 10.1109/TIA.2018.2844804.

[8] O. Gomozov, J. P. F. Trovão, X. Kestelyn, and M. R. Dubois, "Adaptive energy management system based on a real-time model predictive control with nonuniform sampling time for multiple energy storage electric vehicle," *IEEE Trans. Veh. Technol.*, vol. 66, no. 7, pp. 5520–5530, Jul. 2017, doi: 10.1109/TVT.2016.2638912.

[9] S. Zhang, Y. Luo, J. Wang, X. Wang, and K. Li, "Predictive energy management strategy for fully electric vehicles based on preceding vehicle movement," *IEEE Trans. Intell. Transp. Syst.*, vol. 18, no. 11, pp. 3049–3060, Nov. 2017, doi: 10.1109/TITS.2017.2672542.

[10] W. Deng, Y. Zhao, and J. Wu, "Energy efficiency improvement via bus voltage control of inverter for electric vehicles," *IEEE Trans. Veh. Technol.*, vol. 66, no. 2, pp. 1063–1073, Feb. 2017, doi: 10.1109/TVT.2016.2555990.

[11] V. Ruuskanen, J. Nerg, M. Rilla, and J. Pyrhönen, "Iron loss analysis of the permanent-magnet synchronous machine based on finite-element analysis over the electrical vehicle drive cycle," *IEEE Trans. Ind. Electron.*, vol. 63, no. 7, pp. 4129–4136, Jul. 2016, doi: 10.1109/TIE.2016.2549005.

[12] A. G. Sarigiannidis, M. E. Beniakar, and A. G. Kladas, "Fast adaptive evolutionary PM traction motor optimization based on electric vehicle drive cycle," *IEEE Trans. Veh. Technol.*, vol. 66, no. 7, pp. 5762–5774, Jul. 2017, doi: 10.1109/TVT.2016.2631161.

[13] D. Tan, H. Xue, K. Yang, A. Li, and H. Wang, "Study on the thermal characteristics of in-wheel motor drive system based on driving cycles," *IEEE Access*, vol. 7, pp. 14463–14471, 2019, doi: 10.1109/ACCESS.2018.2887143.

[14] H. Yeo, H. Park, J. Seo, S. Jung, J. Ro, and H. Jung, "Electromagnetic and thermal analysis of a surface-mounted permanent-magnet motor with overhang structure," *IEEE Trans. Magn.*, vol. 53, no. 6, Jun. 2017, Art. no. 8203304, doi: 10.1109/TMAG.2017.2668462.

[15] J. Lee, H. Yeo, H. Jung, T. Kim, and J. Ro, "Electromagnetic and thermal analysis and design of a novel-structured surface-mounted permanent magnet motor with high-power-density," *IET Electric Power Appl.*, vol. 13, no. 4, pp. 472–478, 2019, doi: 10.1049/iet-epa.2018.5322.

[16] S. Cui, P. Sun, Z. Kuang, and T. Zhao, "A thermal-electromagnetic coupled motor design flow for electric aircraft propeller drive application," in *Proc. IEEE Transp. Electrific. Conf. Expo Asia-Pacific*, Harbin, 2017, pp. 1–6, doi: 10.1109/ITEC-AP.2017.8080980.

[17] G. Zhang, W. Hua, M. Cheng, B. Zhang, and X. Guo, "Coupled magnetic-thermal fields analysis of water cooling flux-switching permanent magnet motors by an axially segmented model," *IEEE Trans. Magn.*, vol. 53, no. 6, Jun. 2017, Art. no. 8106504, doi: 10.1109/TMAG.2017.2668845.

[18] J. Si, S. Zhao, H. Feng, Y. Hu, and W. Cao, "Analysis of temperature field for a surface-mounted and interior permanent magnet synchronous motor adopting magnetic-thermal coupling method," *CES Trans. Elect. Machines Syst.*, vol. 2, no. 1, pp. 166–174, Mar. 2018, doi: 10.23919/TEMS.2018.8326464.

[19] Y. Chen, X. Zhu, L. Quan, and L. Wang, "Performance analysis of a double-salient permanent-magnet double-rotor motor using electromagnetic–thermal coupling method," *IEEE Trans. Appl. Supercond.*, vol. 26, no. 4, Jun. 2016, Art. no. 5205305, doi: 10.1109/TASC.2016.2543598.

[20] X. Yang, Y. Liu, and L. Wang, "An improved analytical model of permanent magnet eddy current magnetic coupler based on electromagnetic-thermal coupling," *IEEE Access*, vol. 8, pp. 95235–95250, 2020, doi: 10.1109/ACCESS.2020.2995652.

[21] S. Mukundan, H. Dhulipati, J. Tjong, and N. C. Kar, "Parameter determination of PMSM using coupled electromagnetic and thermal model incorporating current harmonics," *IEEE Trans. Magn.*, vol. 54, no. 11, Nov. 2018, Art. no. 8110505, doi: 10.1109/TMAG.2018.2837087.

[22] S. Hwang, J. Chin, and M. Lim, "Design process and verification of SPMSM for a wearable robot considering thermal characteristics through LPTN," *IEEE/ASME Trans. Mechatronics*, vol. 26, no. 2, pp. 1033–1042, Apr. 2021, doi: 10.1109/TMECH.2020.3015561.

[23] J. Chin, S. Hwang, H. Park, and J. Hong, "Thermal analysis and verification of PMSM using LPTN considering mechanical components and losses," in *Proc. 13th Int. Conf. Elect. Mach.*, Alexandroupoli, 2018, pp. 1323–1329, doi: 10.1109/ICELMACH.2018.8507164.

[24] Y. Wang, D. M. Ionel, and D. Staton, "Ultrafast steady-state multi-physics model for PM and synchronous reluctance machines," *IEEE Trans. Ind. Appl.*, vol. 51, no. 5, pp. 3639–3646, Sep./Oct. 2015, doi: 10.1109/TIA.2015.2420623.

Authorized licensed use limited to: Hanyang University. Downloaded on June 17,2021 at 08:59:40 UTC from IEEE Xplore. Restrictions apply.

[25] B. Lee, K. Kim, J. Jung, J. Hong, and Y. Kim, "Temperature estimation of IPMSM using thermal equivalent circuit," *IEEE Trans. Magn.*, vol. 48, no. 11, pp. 2949–2952, Nov. 2012, doi: 10.1109/TMAG.2012.2196503.
[26] M. Gulec, M. Aydin, J. Nerg, P. Lindh, and J. Pyrhonen, "Magneto-Thermal analysis of an axial-flux permanent-magnet-assisted eddy-current brake at high-temperature working conditions," *IEEE Trans. Ind. Electron.*, vol. 68, no. 5, pp. 5112–5121, Jun. 2021, doi: 10.1109/TIE.2020.2992020.
[27] F. Xie, W. Hong, W. Wu, K. Liang, and C. Qiu, "Current distribution method of induction motor for electric vehicle in whole speed range based on gaussian process," *IEEE Access*, vol. 7, pp. 165974–165984, 2019, doi: 10.1109/ACCESS.2019.2953293.
[28] A. M. Aljehaimi, and P. Pillay, "Novel flux linkage estimation algorithm for a variable flux PMSM," *IEEE Trans. Ind. Appl.*, vol. 54, no. 3, pp. 2319–2335, May/Jun. 2018, doi: 10.1109/TIA.2018.2794338.
[29] S. Xiao, and A. Griffo, "PWM-Based flux linkage and rotor temperature estimations for permanent magnet synchronous machines," *IEEE Trans. Power Electron.*, vol. 35, no. 6, pp. 6061–6069, Jun. 2020, doi: 10.1109/TPEL.2019.2948578.
[30] H. Kim, J. Jeong, M. Yoon, J. Moon, and J. Hong, "Simple size determination of permanent-magnet synchronous machines," *IEEE Trans. Ind. Electron.*, vol. 64, no. 10, pp. 7972–7983, Oct. 2017.
[31] S. Park, J. Park, S. Hwang, J. Kim, H. Park, and M. Lim, "Suppression of torque ripple caused by misalignment of the gearbox by using harmonic current injection method," *IEEE/ASME Trans. Mech.*, vol. 25, no. 4, pp. 1990–1999, Aug. 2020.
[32] B. Gallert, G. Choi, K. Lee, X. Jing, and Y. Son, "Maximum efficiency control strategy of PM traction machine drives in GM hybrid and electric vehicles," in *Proc. IEEE Energy Convers. Congr. Expo.*, Cincinnati, OH, USA, 2017, pp. 566–571, doi: 10.1109/ECCE.2017.8095833.
[33] B. Lee, S. Kwon, T. Sun, J. Hong, G. Lee, and J. Hur, "Modeling of core loss resistance for *d-q* equivalent circuit analysis of IPMSM considering harmonic linkage flux," *IEEE Trans. Magn.*, vol. 47, no. 5, pp. 1066–1069, May 2011, doi: 10.1109/TMAG.2010.2099647.
[34] P. H. Mellor, D. Roberts, and D. R. Turner, "Lumped parameter thermal model for electrical machines of TEFC design," *IEE Proc. Electric Power Appl.*, vol. 138, no. 5, pp. 205–218, Sep. 1991, doi: 10.1049/ip-b.1991.0025.
[35] C. Kim, and K. Lee, "Thermal nexus model for the thermal characteristic analysis of an open-type air-cooled induction motor," *Appl. Thermal Eng.*, vol. 112, pp. 1108–1116, Feb. 2017, doi: 10.1016/j.applthermaleng.2016.10.197.
[36] A. Boglietti, M. Cossale, M. Popescu, and D. A. Staton, "Electrical machines thermal model: Advanced calibration techniques," *IEEE Trans. Ind. Appl.*, vol. 55, no. 3, pp. 2620–2628, May/Jun. 2019, doi: 10.1109/TIA.2019.2897264.
[37] O. Wallscheid, and J. Böcker, "Global identification of a low-order lumped-parameter thermal network for permanent magnet synchronous motors," *IEEE Trans. Energy Convers.*, vol. 31, no. 1, pp. 354–365, Mar. 2016, doi: 10.1109/TEC.2015.2473673.
[38] S. Sashidhar, and B. G. Fernandes, "A novel ferrite SMDS spoke-type BLDC motor for PV bore-well submersible water pumps," *IEEE Trans. Ind. Electron.*, vol. 64, no. 1, pp. 104–114, Jan. 2017, doi: 10.1109/TIE.2016.2609841.
[39] A. Cavagnino, A. Tenconi, and S. Vaschetto, "Experimental characterization of a belt-driven multiphase induction machine for 48-V automotive applications: Losses and temperatures assessments," *IEEE Trans. Ind. Appl.*, vol. 52, no. 2, pp. 1321–1330, Mar./Apr. 2016, doi: 10.1109/TIA.2015.2487456.
[40] S. Utegenova *et al.*, "An investigation into the coupling of magnetic and thermal analysis for a wound-rotor synchronous machine," *IEEE Trans. Ind. Electron.*, vol. 65, no. 4, pp. 3406–3416, Apr. 2018, doi: 10.1109/TIE.2017.2756597.
[41] Y. Wang, D. M. Ionel, and D. Staton, "Ultrafast steady-state multiphysics model for PM and synchronous reluctance machines," *IEEE Trans. Ind. Appl.*, vol. 51, no. 5, pp. 3639–3646, Sep./Oct. 2015, doi: 10.1109/TIA.2015.2420623.
[42] K. Yamazaki, and Y. Kanou, "Rotor loss analysis of interior permanent magnet motors using combination of 2-D and 3-D finite element method," *IEEE Trans. Magn.*, vol. 45, no. 3, pp. 1772–1775, Mar. 2009, doi: 10.1109/TMAG.2009.2012817.
[43] S. Zhang, P. Zheng, B. Yu, L. Cheng, and M. Wang, "Thermal analysis and experimental verification of a staggered-teeth transverse-flux permanent-magnet linear machine," *IET Electric Power Appl.*, vol. 12, no. 7, pp. 1048–1057, Aug. 2018, doi: 10.1049/iet-epa.2017.0828.
[44] N. Simpson, R. Wrobel, and P. H. Mellor, "Estimation of equivalent thermal parameters of impregnated electrical windings," *IEEE Trans. Ind. Appl.*, vol. 49, no. 6, pp. 2505–2515, Nov./Dec. 2013, doi: 10.1109/TIA.2013.2263271.
[45] O. Wallscheid, and J. Böcker, "Design and identification of a lumped-parameter thermal network for permanent magnet synchronous motors based on heat transfer theory and particle swarm optimisation," in *Proc. 17th Eur. Conf. Power Electron. Appl.*, Geneva, Switzerland, 2015, pp. 1–10, doi: 10.1109/EPE.2015.7311718.
[46] S. Rezazade, M. Changizian, A. Saleki, and H. Moghbeli, "Investigation and comparison between PHEV and SHEV for sedan vehicle based on ADVISOR," in *Proc. 9th Annu. Power Electron. Drives Syst. Technol. Conf.*, Tehran, Iran, 2018, pp. 404–409, doi: 10.1109/PEDSTC.2018.8343831.

Sung-Woo Hwang received the bachelor's degree in 2013 in mechanical engineering from Hanyang University, Seoul, South Korea, where he is currently working toward the Ph.D. degree in automotive engineering. His research interests include practical approaches to electric machine design for automotive and robot applications.

Jun-Yeol Ryu received the bachelor's degree in 2016 in mechanical engineering and electronic systems engineering from Hanyang University, Seoul, South Korea, where he is currently working toward the Ph.D. degree in automotive engineering. His research interests include the design and optimization of electric machines and analysis of electro-magnetic field.

Jun-Woo Chin received the bachelor's degree in 2014 in mechanical engineering from Hanyang University, Seoul, South Korea, where he is currently working toward the Ph.D. degree in automotive engineering. His research interests include the design of electric machines and loss and thermal analysis of electric motor and generator.

Soo-Hwan Park received the bachelor's degree in mechanical engineering from Hanyang University, Seoul, South Korea, where he is currently working toward the Ph.D. degree in automotive engineering. From 2019 to 2020, he was with the Korea Institute of Industrial Technology, Goryeong County, South Korea. His main research interests include electromagnetic field analysis, design and optimization of electric machines for automotive and robotics applications, and electric machine drive for industrial applications.

Authorized licensed use limited to: Hanyang University. Downloaded on June 17,2021 at 08:59:40 UTC from IEEE Xplore. Restrictions apply.

Dae-Kee Kim received the bachelor's degree in 2014 in mechanical engineering from Hanyang University, Seoul, South Korea, where he is currently working toward the Ph.D. degree in automotive engineering. His research interests include the design and optimization of electric machines and analysis of vibration generated by electric machines.

Myung-Seop Lim (Member, IEEE) received the bachelor's degree in mechanical engineering, and the master's and Ph.D. degree in automotive engineering from Hanyang University, Seoul, South Korea, in 2012, 2014, and 2017, respectively. From 2017 to 2018, he was a Research Engineer with Hyundai Mobis, Yongin, South Korea. From 2018 to 2019, he was an Assistance Professor with Yeungnam University, Daegu, South Korea. Since 2019, he has been with Hanyang University, where he is currently an Assistant Professor. His research interests include electromagnetic field analysis and multiphysics analysis of electric machinery for mechatronics systems which include automotive and robot applications.

Authorized licensed use limited to: Hanyang University. Downloaded on June 17,2021 at 08:59:40 UTC from IEEE Xplore. Restrictions apply.